Non-Intrusive Item Authentication with High Robustness for RFID-Enabled Logistics

Jiawei Xue*, Chunhui Duan*✉, Fan Li*, Qihua Feng*, Ziang Wang* and Yinan Zhu†
*School of Computer Science and Technology, Beijing Institute of Technology, China
†Department of Computer Science and Engineering, Hong Kong University of Science and Technology, China
Email: {xuejw, duanch, fli, fengqh, ziangwang}@bit.edu.cn, yzhudf@cse.ust.hk

IEEE INFOCOM 2025 - IEEE Conference on Computer Communications | 979-8-3315-4305-1/25/$31.00 ©2025 IEEE | DOI: 10.1109/INFOCOM55648.2025.11044445

***Abstract*—RFID technology has found extensive applications in the realm of smart logistics, facilitating rapid package sorting and tracking. Harnessing the potential of RFID in addressing concerns related to logistics security holds significant promise and meaning. Past efforts either focused solely on the status of tags or package boxes, or interfered with the normal logistics processes. To detect the status of goods inside the packages and provide timely alerts for instances of loss, replacement, or damage, we propose RF-Express, a non-intrusive and anti-interference item authentication method. RF-Express enables seamless authentication of items during the logistics process, utilizing the pervasive RFIDs with almost no additional costs. Specifically, by tactfully arranging a pair of tags on each package and extracting representative features from the backscatter signals of the tags, we manage to discern the authenticity of the item with high precision across various multipath environments. Besides, a feature matching algorithm based on the triplet network is employed to further reinforce the robustness of the system. We implemented the RF-Express prototype on commercial devices and conducted plenty of experiments. It is demonstrated that RF-Express achieves a true acceptance rate of 94.97% and a true rejection rate of 94.38% on average under common attack scenarios.**

***Index Terms*—RFID, Wireless Sensing, Item authentication**

I. Introduction

Motivation. Nowadays, online shopping has become the mainstream mode of shopping for many individuals. Products purchased online are delivered to customers via express services. Generally, express packages go through multiple transit points before reaching their destination. It is challenging to ensure the safety of all transit processes, as incidents of damaged, lost, or replaced goods can occur during the express transportation [1]–[3]. Therefore, conducting status monitoring of goods in the logistics process is crucial to enable logistics companies to promptly detect changes in the package's condition.

In recent years, Radio-Frequency Identification (RFID) technology has found extensive applications in the supply chain and logistics domains, for instance, providing convenient item registration and transportation data recording. Additionally, past efforts have also attempted to provide monitoring services during logistics using RFID, such as authenticating the legitimacy of item tags [4], [5] or wrapping RFID antennas around packages to determine whether they have been tampered with [6]. However, the primary focuses of these methods have been on the authenticity of the tag or the state of the package itself, rather than the condition of the item inside the package. Additionally, the work [7] manages to extract unique features from backscatter signals penetrating the internal space of package to assess the status of item within. Nevertheless, this approach requires dedicated equipment like USRP and is constrained to situations where packages are stationary.

✉Chunhui Duan is the corresponding author.

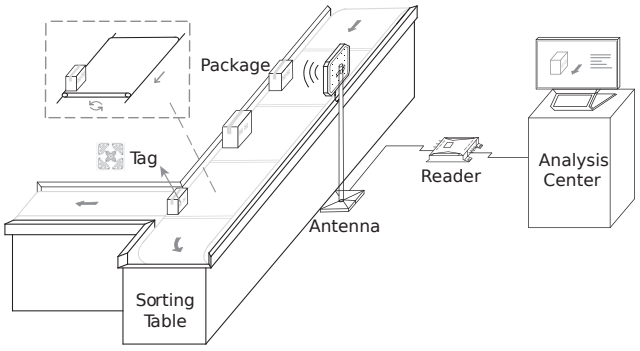

Fig. 1: Overview of the RF-Express operating scenario.

Our Scheme. To facilitate item monitoring in the logistics process, we introduce RF-Express, a non-intrusive and effective item authentication system with purely Commercial Off-The-Shelf (COTS) devices. As depicted in Fig. 1, RFID tags affixed to packages store data that enables rapid package identification by the reader. At sorting nodes, the system directs packages to different downstream nodes based on the stored sorting information. Simultaneously with scanning tags' identities, RF-Express collects and models the backscatter signals from the deployed tags. When the reader antenna communicates with a tag, the wireless signal would be reflected by the item within the tagged package. Besides, different items or the same item in different status (intact or damaged) have unique effects on these signals. To be specific, RF-Express extracts representative signal features from tags at the upstream nodes and registers such feature information. When sorting packages at the downstream nodes, it employs the same method to capture the tag's reflection signals, acquire features, and compare them with the registered ones.

RF-Express leverages the uniform motion of packages to gather backscatter signals from tags at different locations,

obtaining a wealth of data and using it to construct more refined features that precisely reflect item status. Under the system's configuration, at the sorting table, packages move along with the conveyor belt on the side opposite to the reader antenna. Consequently, across various logistics nodes, it is reasonable to assume that the vertical distance from the conveyor to the reader antenna remains nearly constant. For convenience, the rest of this paper will jointly refer to different items or the same item in different status as *different items*.

Challenges and Solutions. To establish a non-intrusive and stable item authentication system, we need to address the following technical challenges.

The first challenge is how to characterize the underlying relationship between the item within the package and the collected RF signals. We theoretically deduce that the backscatter signals of the tag on the package are directly related to the item contained, based on the principles of electromagnetic propagation. To be more specific, it is validated that the item's material type and depth of each layer of medium, as well as the shape of the item, would exert an influence on the amplitude and phase of the received signal.

The second challenge is how to minimize the adverse impact of indoor multipath itself and its variations as well. We propose a cost-effective strategy by properly deploying a pair of RFID tags on each package. By taking the difference of the signals from these two tags when they pass through the same location, we successfully handle the undesirable effect of environmental changes. Besides, a triplet network based feature matching method is utilized to introduce a mechanism of expanding training data, which further overcomes the interference from dynamic multipath. Thus, both the precision and reliability of our system are dramatically improved.

The third challenge is how to handle the inconsistent signal data lengths between upstream and downstream nodes caused by diversities in hardware devices and other factors. Leveraging the fact that the packages are in a moving manner along with the conveyor, an adequate amount of time-varying signals can be acquired for authentication. Then we devise a series of practical techniques for selecting useful signal segments and interpolating original misaligned data so as to extract item-related features effectively.

Contributions. The main contributions of this work are:

(i) To the best of our knowledge, this is the first non-intrusive and anti-interference endeavor in package item authentication utilizing RFID technology. We collect the backscatter signals from the attached tags, which, after processing, serve as unique features to characterize the items.

(ii) To enhance the accuracy and robustness of our approach, we propose the idea of signal differentiation of dual tags, feature extraction under moving conditions, along with a feature matching algorithm incorporating neural network, to surmount impacts brought by factors other than the item itself.

(iii) We implement a prototype system for RF-Express with COTS RFID devices and evaluate its performance with extensive experiments. The results indicate that the system achieves a true acceptance rate of 90.97% and a true rejection rate of 94.38% on average, demonstrating its suitability for the majority of practical applications in smart logistics.

II. Item Feature Extraction

A. Signal Propagation Model

Wireless signals experience a certain degree of attenuation during propagation. Let the signal at the time of transmission be denoted as $S = \alpha e^{\mathbf{J}\theta}$, where α and θ represent the signal's magnitude and phase, while $\mathbf{J}$ denotes the imaginary number. The signal S' arriving at the destination after propagation can be expressed as [8]:

$$S' = h \cdot S, \tag{1}$$

where h is the channel parameter of the transmission. h can also be expressed in the form of $ae^{-\mathbf{J}\Delta\theta}$, where a and $\Delta\theta$ represent the channel attenuation and phase rotation of the signal, respectively.

As shown in Fig. 2a, in the package sorting scenario, the tag receives three main components of the radio-frequency signal: the signal $S_{A\to T}$ directly transmitted by the reader antenna to the tag, the signal $S_{A\to E\to T}$ reflected by environmental reflectors to the tag, and the signal $S_{A\to P\to T}$ that reaches the tag after being reflected by the item inside the package. Let S_0 be the signal sent from the antenna. The signal arriving at the tag can be represented as:

$$\begin{aligned} S_T &= (S_{A\to T} + S_{A\to E\to T} + S_{A\to P\to T}) \cdot h_T \\ &= (h_{A\to T} + h_{A\to E\to T} + h_{A\to P\to T}) \cdot S_0 \cdot h_T. \end{aligned} \tag{2}$$

Here h_T represents the signal change caused by the tag itself. We use h_A to denote the signal change introduced by the reader antenna. Then the signal returning to the antenna can be described as below:

$$S_{T\to A} = h_A \cdot h_{T\to A} \cdot S_T. \tag{3}$$

B. Channel Parameters

$h_{A\to T}(= h_{T\to A})$ and $h_{A\to E\to T}$ are respectively related to the distance from tag to reader antenna and the surrounding environment. Before analyzing $h_{A\to P\to T}$, we introduce some preliminary knowledge about signal refraction and reflection. As indicated within the circle in Fig. 2b, when a signal pass from one medium m_a into another medium m_b, at the interface, it is divided into two parts: one part is reflected back into the original medium, and the other part undergoes refraction, passing through the surface into the new medium [9]. The propagation of signal at the interface of the two mediums is closely related to the dielectric constants of the two mediums and the angle of incidence of the signal with respect to the normal. For the sake of clarity in subsequent explanations, we denote the dielectric constants of the original medium and the new medium as two complex numbers ϵ_{ra} and ϵ_{rb}, and the angle between the signal's arrival at the interface and the normal as φ_{inc}.

Signal Refraction: After the signal enters the new medium, its propagation direction changes due to refraction. Let's define the angle between the signal and the normal line within

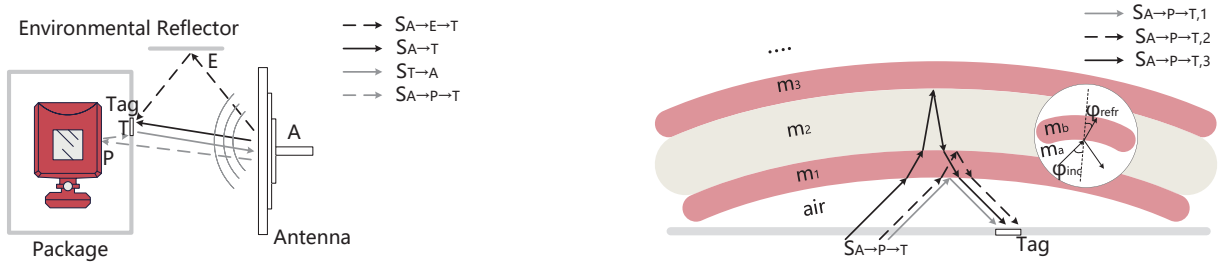

(a) The signals transmitted from the reader antenna reach the tag through multiple paths.

(b) The signals reach the surface of the item, undergo refraction and reflection, and then reach the tag.

Fig. 2: Radio frequency signal propagation model.

medium m_b after refraction as φ_{refr}. The relationship between φ_{refr} and the angle of incidence φ_{inc} can be expressed as [9]:

$$\text{Re}(\sqrt{\epsilon_{ra}})\sin\varphi_{\text{inc}} = \text{Re}(\sqrt{\epsilon_{rb}})\sin\varphi_{\text{refr}}, \tag{4}$$

where $\text{Re}(\cdot)$ denotes taking the real part of a complex number. The angle φ_{inc} depends on the signal's propagation direction and is also influenced by the shape of the new medium. When signal propagates within a medium with a relatively large dielectric constant, amplitude attenuation occurs. Let the depth of the new medium be denoted as d_b. We can define the channel parameter for the signal passing through the new medium m_b as:

$$h_b = \frac{1}{d_b} e^{-\mathbf{J}2\pi f \frac{d_b\sqrt{\epsilon_{rb}}}{c}}. \tag{5}$$

Let us represent $\sqrt{\epsilon_{rb}}$ in the complex form as $\boldsymbol{\alpha} - \boldsymbol{\beta}\mathbf{J}$, and the channel parameter h_b can then be represented as:

$$h_b = \frac{1}{d_b} e^{-2\pi f \frac{d_b\boldsymbol{\beta}}{c}} e^{-\mathbf{J}2\pi f \frac{d_b\boldsymbol{\alpha}}{c}}. \tag{6}$$

The real value $\frac{1}{d_b} e^{-2\pi f \frac{d_b\boldsymbol{\beta}}{c}}$ characterizes the amplitude attenuation of the signal, affecting its power. The imaginary value $e^{-\mathbf{J}2\pi f \frac{d_b\boldsymbol{\alpha}}{c}}$ represents the phase variation of the signal.

Signal Reflection: When the signal undergoes reflection at the medium interface, there is a certain degree of power loss, and the phase may also experience rotation. According to [10], [11], we can define the channel parameter for the signal during reflection by the following equation:

$$h_{\text{refl},a\to b\to a} = \sqrt{R_{\text{refl}}} \cdot e^{-\mathbf{J}\theta_{\text{refl}}}, \tag{7}$$

where R_{refl} is the power reflection coefficient:

$$\begin{aligned} R_{\text{refl}} = &\left| \frac{\sqrt{\epsilon_{rb}}\cos\varphi_{\text{refr}} - \sqrt{\epsilon_{ra}}\cos\varphi_{\text{inc}}}{\sqrt{\epsilon_{rb}}\cos\varphi_{\text{refr}} + \sqrt{\epsilon_{ra}}\cos\varphi_{\text{inc}}} \right|^2 \\ &\times \left| \frac{\sqrt{\epsilon_{rb}}\cos\varphi_{\text{inc}} - \sqrt{\epsilon_{ra}}\cos\varphi_{\text{refr}}}{\sqrt{\epsilon_{rb}}\cos\varphi_{\text{inc}} + \sqrt{\epsilon_{ra}}\cos\varphi_{\text{refr}}} \right|^2, \end{aligned} \tag{8}$$

and θ_{refl} is the potential phase shift:

$$\theta_{\text{refl}} = \begin{cases} 0, & \varphi_{\text{inc}} \le \varphi_B \\ \pi, & \varphi_{\text{inc}} > \varphi_B \end{cases}, \quad \varphi_B = \arctan\sqrt{\frac{\epsilon_{rb}}{\epsilon_{ra}}}. \tag{9}$$

The items generally consist of multiple layers of materials. For ease of description, in Fig. 2b, we depict the signals passing through refraction, ultimately reaching the surface of medium m_3, then escaping from the item through reflection and refraction. Without loss of generality, we analyze that the signals can reach the interface between the M^{th} layer medium m_M and the $(M+1)^{\text{th}}$ layer medium m_{M+1}, and then undergo reflection and escape back into the air. The signals reflected from the item can be considered as being composed of $M+1$ reflected signals. Then we can compute $h_{A\to P\to T}$ as:

$$h_{A\to P\to T} = \sum_{i=1}^{M+1} h_{A\to P\to T,i} = \sum_{i=1}^{M+1} h_{A\to P,i}\cdot h_{P,i}\cdot h_{P\to T,i}. \tag{10}$$

Here $h_{A\to P,i}$ and $h_{P\to T,i}$ respectively represent the channel parameters from the reader antenna to the item and from the item to the tag. $h_{P,i}$ denotes the change in the signal that travels to the surface of medium m_i and then returns, undergoing reflection from the i^{th} layer and refraction through $i-1$ layers of medium. We have:

$$h_{P,i} = h_{\text{refl},i-1\to i\to i-1} \prod_{j=1}^{i-1} h_j \prod_{j=1}^{i-1} h'_j, \tag{11}$$

where h_j and h'_j denote the channel parameters for the signal passing through medium m_j on two different occasions, before and after. Combining Eqn. 4, Eqn. 6 and Eqn. 7, it can be observed that the channel parameter $h_{P,i}$ depends on the material type and depth of each layer of medium that the signal passes through, as well as the shape of the reflected region.

In summary, incorporating Eqn. 3, if the direct path ($h_{A\to T}$ and $h_{T\to A}$) and environmental multipath ($h_{A\to E\to T}$) keep stable, the signal received by the reader $S_{T\to A}$ will inevitably change with variations in the item inside the package. Additionally, as the package moves, the region on the item where the signal is reflected back to the tag will also shift. We will provide a detailed explanation of this in Section II-D.

C. Dealing with Multipath Variations

Since the registration and authentication are performed at different nodes whose surrounding environment could be quite dissimilar, the system will experience variations in environmental multipath reflections. In order to guarantee the accuracy of RF-Express, it is crucial to deal with the negative impact from the multipath variations. Instead of identifying a package

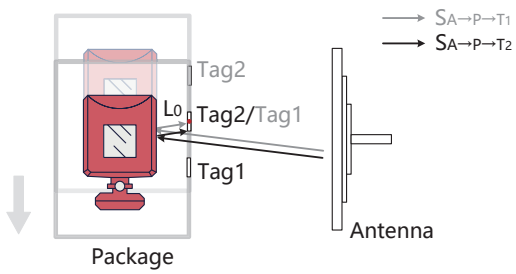

Fig. 3: As the package moves in the direction of the arrow, Tag2 will pass through the same positions as Tag1.

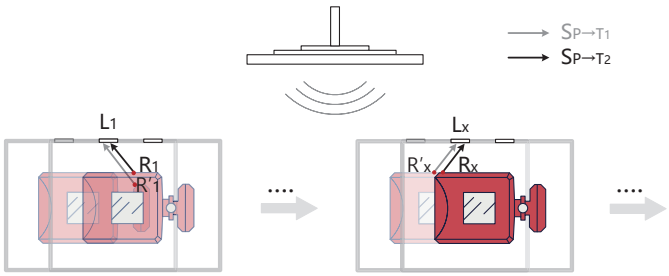

Fig. 4: When Tag1 and Tag2 pass through point L_x successively, signals are reflected from the regions R'_x and R_x of the item to the tags, respectively.

by a single tag, we come up with a solution by tactfully introducing an extra tag, namely affixing a pair of tags on each package. The dual tags are located on the same surface of the package, in a parallel way, with one sitting in front (referred as *leading tag*) and the other in back (referred as *trailing tag*). When the package moves, the trailing tag will pass through the same positions as the leading tag. As shown in Fig. 3, Tag1 first reaches position L_0 (indicated by the red dot). As the package moves in the direction of the arrow, Tag2 will subsequently reach position L_0 as well.

Let $S_{T_1\to A,L_0}$ and $S_{T_2\to A,L_0}$ denote the signals reflected back to the reader by Tag1 and Tag2, respectively, at position L_0. Their compositions can be referred to Eqn. 2 and Eqn. 3. We assume the two tags are from the same brand and batch, and thus have negligible hardware differences. The relative positions of the two tags at L_0 with respect to the antenna are the same, and the multipath reflections in the environment at L_0 are also the same:

$$\begin{aligned} &S_{T_1\to A,L_0} - S_{T_2\to A,L_0} \\ &= h(S_{A\to T_1,L_0} + S_{A\to E\to T_1,L_0} + S_{A\to P\to T_1,L_0}) \\ &\quad - h(S_{A\to T_2,L_0} + S_{A\to E\to T_2,L_0} + S_{A\to P\to T_2,L_0}) \\ &\approx h(S_{A\to P\to T_1,L_0} - S_{A\to P\to T_2,L_0}). \end{aligned} \tag{12}$$

Here h is the hardware parameter. Since Tag1 and Tag2 have different reflection points on the item at L_0, subtracting $S_{T_2\to A}$ from $S_{T_1\to A}$ preserves the reflection signals from the item.

D. Feature Extraction Under Movement

So far, we have analyzed the impact of different items inside the package on the tag's backscatter signal and introduced how to mitigate the effects of multipath changes through properly arranging a pair of tags on each package. Remember here we have a premise that the package is in a moving condition, which is also the application scenario of RF-Express.

As illustrated in Fig. 4, in our sampled data, we denote the same position where Tag1 and Tag2 are located for the x^{th} timeslot as L_x. At L_x, signals from the region R'_x and region R_x of the item are reflected to Tag1 and Tag2, respectively. By taking the difference between the backscatter signals of the two tags at position L_x, we can obtain the difference between the signals reflected from the region R'_x and region R_x. Let's denote that there are a total of N such points in our samples where both Tag1 and Tag2 have reflected signals at or near those points. In this case, each tag has N valid signal samples: $[S_{T_1\to A,L_1}, S_{T_1\to A,L_2}, \ldots, S_{T_1\to A,L_N}]$ and $[S_{T_2\to A,L_1}, S_{T_2\to A,L_2}, \ldots, S_{T_2\to A,L_N}]$. The corresponding regions reflected from the item are: $\boldsymbol{R'} = [R'_1, R'_2, \ldots, R'_N]$ and $\boldsymbol{R} = [R_1, R_2, \ldots, R_N]$. The signal difference sequence obtained by subtracting the signal samples of the two tags, $[\Delta S_{L_1}, \Delta S_{L_2}, \ldots, \Delta S_{L_N}]$, will be weakly correlated with environmental factors but strongly correlated with $\boldsymbol{R'}$ and $\boldsymbol{R}$.

The signals from the two tags collected by the reader at the same time come from different positions. If we can align the two tags' signal samples from the same position, the obtained difference will well reflect the material composition and shape of different regions of the item.

III. System Design

A. Overview

RF-Express is composed of three main parts: *signal acquisition*, *data preprocessing* and *feature matching*. In the signal acquisition module, the system collects reflection signals from dual tags and extracts phase and RSSI data. Subsequently, the signal data undergo alignment using a phase-based V-zone detection method in the data preprocessing module, followed by computation of the signal differentials. In the feature matching module, the computed differentials are paired with corresponding registered upstream differential data from the database and input into a pre-trained network. Finally, RF-Express calculates their feature similarity and compares them with a pre-defined threshold to determine whether the item has changed. We will elaborate on the details of data preprocessing and feature matching in the following sections.

B. Data Preprocessing

1) V-zone Detection: In the application scenario of RF-Express, the package moves uniformly on the conveyor belt from one end to another, and the distance from the tag to the antenna would decrease first and then increases. There exists a linear relationship between the reported phase and distance as described in Eqn. 13:

$$\theta = (\frac{2\pi f}{c} \times 2d + \theta_{\text{refl}} + \theta_{\text{hdw}}) \bmod 2\pi, \tag{13}$$

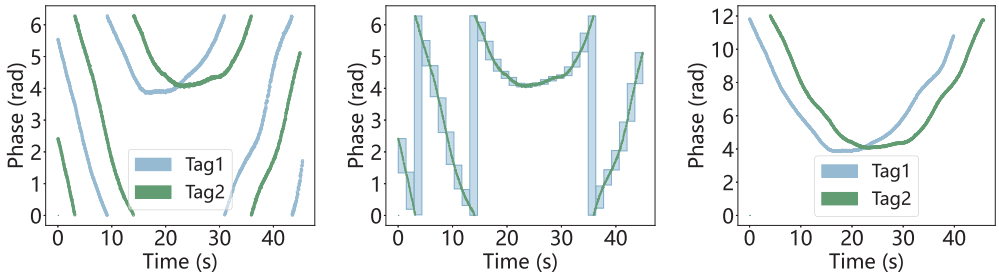

(a) Original sequence (b) Sliding window (c) Concatenated sequence

Fig. 5: The acquired phase sequences.

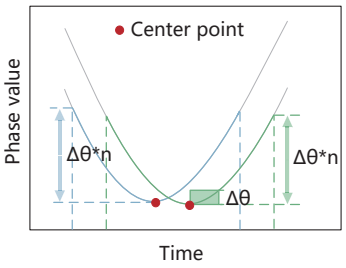

Fig. 6: Signal selection based on the sliding window.

where θ_{refl} and θ_{hdw} represent the phase offsets caused by reflection and hardware, respectively. Although these offsets affect the phase values, they do not influence the trend of phase variation with distance. Hence, the phase value would also first decrease and then increase with distance, forming a distribution shaped like the letter 'V', called as V-zone for convenience. Therefore, if we identify the V-zones in the phase sequences of two tags, we can deduce which signal samples from the two tags come from the same position or adjacent positions. However, in reality, the obtained phase values are modulo data, causing the V-shaped phase to be segmented into small sections, as shown in Fig. 5a.

To address this, we employ a signal splicing and V-zone detection method [12]. Let the phase sequence be $\mathbf{\Theta} = [\theta_0, \theta_1, \ldots, \theta_{K-1}]$. As shown in Fig. 5b, we use a sliding window of length w to divide the sequence into $\frac{K}{w}$ sub-sequences $\mathbf{\Theta} = [\Theta_0, \Theta_1, \ldots, \Theta_{\frac{K}{w}-1}]$, where $\Theta_i = [\theta_{iw}, \theta_{iw+1}, \ldots, \theta_{iw+w-1}]$. When the phase sub-sequence Θ_i exhibits the following condition, we consider it as a jump sub-sequence, *i.e.*, a phase jump occurs:

$$\begin{aligned} \max(\Theta_i) - \min(\Theta_i) > \tau \quad \text{or} \\ |\texttt{last}(\Theta_i) - \texttt{first}(\Theta_{i+1})| > \tau. \end{aligned} \tag{14}$$

Here, τ is a manually set jump threshold, $\texttt{last}(\cdot)$ and $\texttt{first}(\cdot)$ denote taking the last and first values of the sequence, respectively. Let the set composed of jump sub-sequences be $\mathbf{\Theta}_{\text{jump}} = [\Theta_{j,1}, \Theta_{j,2}, \ldots, \Theta_{j,S}]$. In a jump sub-sequence $\Theta_{j,i}$, we identify two jump points θ_{j,i_1} and θ_{j,i_2}, representing the last sample point before the signal jump and the first sample point after the signal jump, respectively. The V-zone we are looking for has its ends determined by two jump points from the two consecutive jump sub-sequences, θ_{j,i_2} and $\theta_{j,(i+1)_1}$, and these two jump points have phase values close to 2π. Therefore, if two adjacent jump sub-sequences meeting these criteria are found, the interval between these two jump points is considered a V-zone of the phase sequence:

$$\begin{aligned} 2\pi - \theta_{j,i_2} \leq \eta \quad \text{and} \\ 2\pi - \theta_{j,(i+1)_1} \leq \eta, \end{aligned} \tag{15}$$

where η is also a manually set threshold. Let θ_{j,i_2} and $\theta_{j,(i+1)_1}$ be V_{left} and V_{right}, and they serve as the starting and ending points of the V-zone.

2) Signal Selection: As shown in Fig. 6, we use the center point of the aforementioned V-zone as the starting point for signal selection, with $\Delta\theta$ as the phase span of the sliding window. Starting from the center of the V-zone, we slide respective n windows to the left and right, and all the signal samples passed by each sliding window are saved. $\Delta\theta$ and n are user-defined parameters. Since our sliding window has a fixed phase span, *i.e.*, the phase change corresponding to each window is equal, based on the relationship between distance and phase, each sliding window corresponds to an approximately equal change in the package distance. This way, the selected signal segment corresponds to a fixed communication range. Even if the speed of the conveyor belt varies among different nodes, it will only affect the number of signal samples, and the overall trend of the selected signal segment remains consistent.

3) Data Interpolation: After the processing in Section III-B2, the final selected signal samples for each tag come from the same communication range. To ensure equal sample counts for the dual tags and to maintain consistent data length input to the neural network, we perform interpolation on the data next. To prevent interference from jump values during interpolation, we first concatenate the truncated phase values resulting from the modulo operation. We set a parameter Γ with an initial value of 0. Starting from the center of the V-zone toward both ends, the phase values of all selected sample points increase by Γ. Whenever encountering a jump point, Γ increases by 2π. After concatenation, as we can see in Fig. 5c, the signal phase is now a continuous sequence.

We generate a new time sequence of length N based on the selected signal samples' time sequence. We then use piecewise linear interpolation to interpolate the RSSI sequence and the concatenated phase sequence. After this step, we obtain the new feature sequences for the dual tags, each consisting of an RSSI sequence of length N and a phase sequence of length N. The samples from both tags are derived from the same communication range.

4) Signal Difference Computation: According to Eqn. 16, we convert the RSSI values and phase values (*i.e.*, θ) into a composite signal, represented by the in-phase (I) and quadrature (Q) values [13].

$$S_{T \to A} = \sqrt{10^{RSSI/10-3}} \cdot e^{\mathbf{J}\theta}. \tag{16}$$

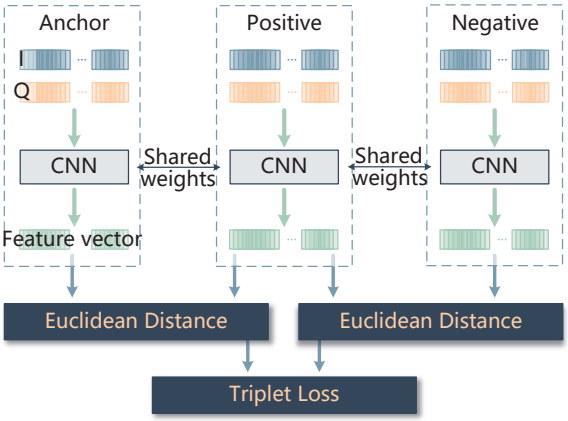

Fig. 7: Training process of the triplet network

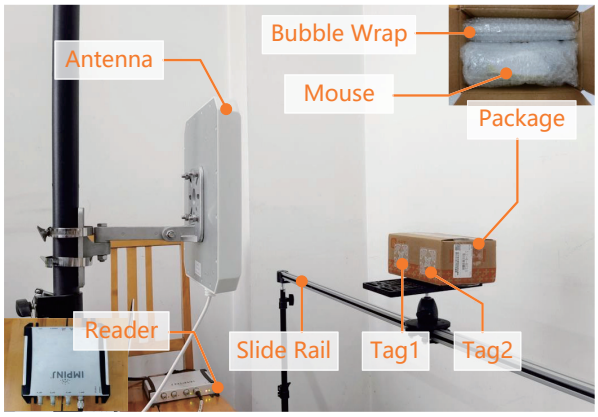

Fig. 8: Experiment setup of RF-Express.

By performing vector subtraction on the aligned dual-tag signals, we obtain the signal difference. This signal difference serves as the sample data for the package, which is input into the network for feature computation.

C. Feature Matching

We use a triplet network [14] for the feature matching. The goal of the matching process is to compute the similarity between two sets of signal samples to determine whether they are signals reflected from the same item. The triplet network is designed to map signal samples from the same item to nearby distances in the feature space, and conversely, to map samples from different items to distant distances [15], [16]. With a trained network, we can calculate the similarity between two sets of signal samples.

The training data for the triplet network is organized in triplets, with two sets of signal data from the same item (anchor sample and positive sample) and one set from another item (negative sample). As Fig. 7 shows, these three sets of samples are input into the same network, resulting in three sets of feature vectors. Then we calculate the Euclidean distances between the feature vectors of the anchor sample and the positive sample, as well as the anchor sample and the negative sample, respectively. These two sets of Euclidean distances will be used to compute the loss. The entire network is optimized by minimizing the triplet loss function $\mathcal{L}$:

$$\mathcal{L} = \sum_{i}^{T} [||f(\Delta S_i^a) - f(\Delta S_i^p)||_2^2 - ||f(\Delta S_i^a) - f(\Delta S_i^n)||_2^2 + \lambda]_+. \tag{17}$$

Here, T represents the number of triplet samples. ΔS_i^a, ΔS_i^p, and ΔS_i^n represent the anchor, positive, and negative samples, respectively. $f(\cdot)$ represents the convolutional neural network. λ is a hyperparameter used to control the distance between positive and negative samples.

During the feature matching process, The input is no longer a triplet but a pair, *i.e.*, the features of the signals collected by the upstream and downstream. We feed these two sets of signal difference data into the trained network, obtaining two sets of feature vectors. Since the system needs to authenticate various types of items, which could be liquids, metals, or glass, it is challenging to determine a Euclidean distance-based threshold. Therefore, unlike the training process, here we express the similarity between two sets of features using *cosine similarity*. We compare this similarity with a pre-set threshold. If the similarity exceeds the threshold, we consider that the two sets of signal difference data correspond to the same item; otherwise, we conclude that the item has changed, and the system issues an alert.

IV. Implementation

A. Prototype

Hardware: RF-Express uses an ImpinJ Speedway Revolution R420 reader, compatible with the EPC Gen2 standard. The reader is connected to the host end via Ethernet. We adopt a circularly polarized antenna Larid S9028PCL with dimensions of $22.5\,\mathrm{cm} \times 22.5\,\mathrm{cm} \times 4\,\mathrm{cm}$ and a gain of $8\,\mathrm{dBi}$. Tags from the ImpinJ Monza H47 model are employed, each with a size of $50\,\mathrm{mm} \times 50\,\mathrm{mm}$.

Software: The host end communicates with the reader through the Low Level Reader Protocol (LLRP) [17]. R420 reader extends this protocol to support RSSI and phase reports. The RF signal acquisition program is implemented in Java, and the data analysis program is implemented in Python. We use an LG laptop with an Intel Core i5 processor and 16GB memory to run all our programs.

System Settings: As shown in Fig. 8, we utilize a photography slide rail to simulate a conveyor belt. The slider can smoothly move at various speeds. A metal plate installed on the slider can support the package box. The reader antenna is positioned approximately $0.45\,\mathrm{m}$ horizontally from the slider. To make the setup more similar to a real express scenario, we include bubble wrap inside the package, which also helps secure the items in the package.

B. Dataset & Network Training

The experiment involves preparing five different liquids (contained in the same type of container), five different models of smartphones, two different models of mice, and two

TABLE I: Description of items used in the experiment.

Usage	Items	Category
Train	Water, Orange juice, Salt soda water	Liquid
	iPhone14Pro, Xiaomi 8, vivo X60Pro	Phone
	Bus building blocks	Blocks
Test	Coca cola, Mulberry juice	Liquid
	iPhone15, OnePlus 9	Phone
	Logitech M330, Logitech PEBBLE	Mouse
	Truck building blocks	Blocks

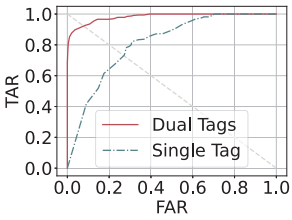

Fig. 9: ROC curves for dual-tag and single-tag cases, with EERs of 7.79% and 27.02% respectively.

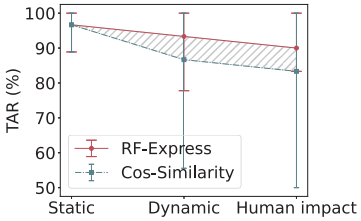

Fig. 10: The TARs of RF-Express and traditional cosine similarity matching method in different environments.

building blocks for data collection. We use different states of building blocks to simulate damage to items. Signal data collected at different times from three of these liquids, three smartphones, and the same building block in three different states will be used to train the network. The remaining items are used to test the system's performance. Their specific details are shown in Table I.

As introduced in Section III-C, data used for training needs to be input to the network in the form of triplets. We expect the network to distinguish between different items, even if they are relatively similar. It is not meaningful to train the network to distinguish between different categories of items. Therefore, anchor samples and negative samples should be different items from the same category. We treat liquids, smartphones, and building blocks as separate category groups, with each group containing three items.

We use PyTorch framework [18] to build the CNN. The Adaptive Moment Estimation (Adam) [19] algorithm based on gradient descent is employed to optimize the network, with a learning rate set to 0.001. The hyperparameter λ in the loss function (Eqn. 17) is set to 0.2 after parameter experiments. The network is trained for 100 epochs.

Feature signals for the remaining items under various settings are collected for testing. These settings include different multipath environments, dynamic influences, antenna-tag distances, item positions, speeds, *etc*. We will elaborate on the authentication performance of the system under these settings in the upcoming evaluation section.

V. Evaluation

In this section, we will present the experimental results of RF-Express. The pairs used for testing are divided into two groups. The first group consists of data collected from the same item at different times (Group#1), referred to as positive samples. The second group comprises signal data from different items (Group#2), labeled as negative samples.

A. Metrics

We define the following three metrics to evaluate RF-Express: True Acceptance Rate (TAR), True Rejection Rate (TRR), and Equal Error Rate (EER). TAR represents the number of correctly accepted pairs divided by the total number of pairs in Group#1. TRR corresponds to the number of correctly rejected pairs divided by the total number of pairs in Group#2. EER is a point on the Receiver Operating Characteristic (ROC) curve, and the ROC curve describes the variation of TAR and False Acceptance Rate (FAR) at different thresholds, with FAR = 1 - TRR. EER is the point where TAR and FAR are equal, representing the system's performance threshold.

B. Performance of Item Authentication

1) Threshold Experiment: We conduct authentication experiments on similar items and analyze the ROC curve. This means that we select signal data from different items of the same category to form negative sample pairs, while positive sample pairs still consist of signal data collected from the same item at different times. As the threshold changes, the ROC curve depicts the variation in TAR and FAR. The trend of TAR and FAR is displayed in the ROC curve graph in Fig. 9. The results indicate that, in the case of attacks involving replacing similar items (items of the same category), the system's EER is 7.79%. To ensure the recognition accuracy of the system in the replacement of similar items, we will assign the threshold determined in this experiment to the system for the subsequent evaluation.

As a comparison, we also depict the ROC curve for the single-tag setting (shown in Fig. 9), where the EER reaches 27.02%. The system's critical performance under this setting is comparatively poor. This demonstrates that the dual-tag method we proposed has largely mitigated the impact of environmental variations, improving the accuracy of the system.

2) Overall Accuracy: We conduct an overall evaluation by simulating situations that may occur in real life, including the replacement of similar items, item loss (empty box), and item damage. We collect signals from various items in nine different environments. The data for the same item in any two distinct environments are respectively used as upstream and downstream samples to evaluate the system's TAR. The data combinations gathered for different items across these nine environments are used to assess the system's TRR. We take the average of the test results for all sample combinations as the final outcome.

Fig. 11a, Fig. 11b and Fig. 11c respectively reveal the TAR of the system for authenticating smartphones, liquids, and mouse items, as well as their TRR when replaced by similar items or lost. Fig. 11d illustrates the TAR and TRR of authentication for blocks in different assembly states. The

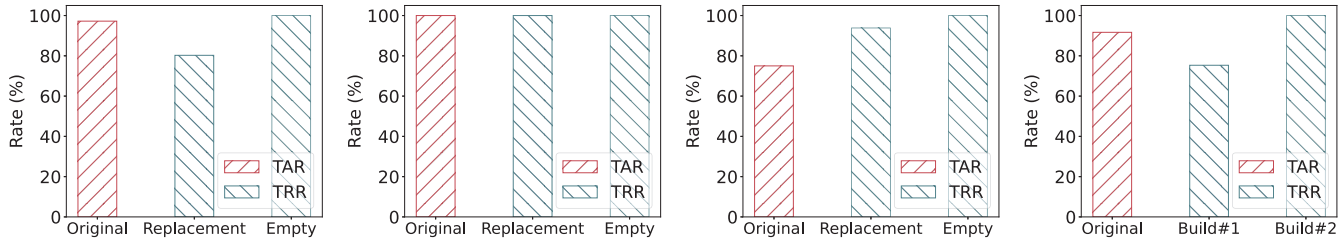

(a) Smartphone (b) Liquid (c) Mouse (d) Blocks

Fig. 11: The authentication accuracy for different types of items.

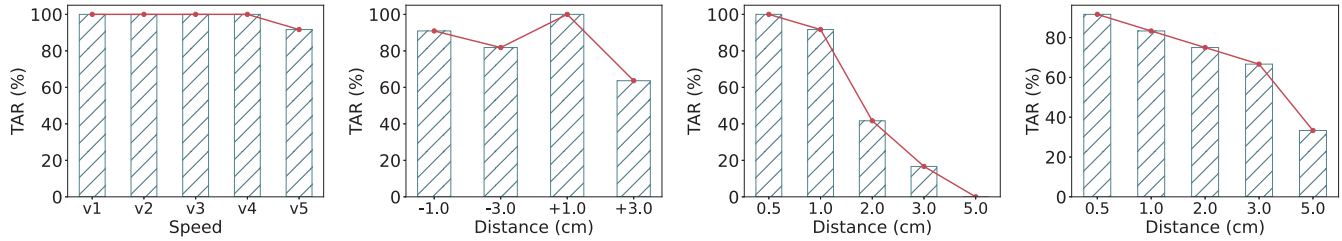

Fig. 12: Impact of Conveyor Speed.

Fig. 13: Impact of Package-Antenna Distance.

Fig. 14: Impact of Item's Lateral Movement.

Fig. 15: Impact of Item's Vertical Movement.

different assembly states of the blocks can simulate the degree of item damage. The results show that RF-Express achieves a TAR of 90.97% for the original items (without replacement, loss, or damage) and a TRR of 94.38% for items with changed states. Specifically, the recognition rate for item loss is 100%, for similar item replacement is 91.36%, and for damaged items, it is 91.77% (depending on the degree of damage; the variation in building#2 in the figure is more significant).

3) Impact of Different Environmental Changes: We collect signal data for the same item in different environments and evaluate the system's TAR. We introduce different multipath reflections in the static environment. The dynamic environments include two typical scenarios: one with reflective objects moving along with the guide rail, simulating other goods on the conveyor belt, and the other with people walking around the guide rail.

Fig. 10 presents our experimental results. For static environment where multipath changes, both RF-Express and the traditional cosine similarity matching method achieve a TAR of 96.67%. In dynamic multipath changes and scenarios with multiple people moving around the system, RF-Express achieves TARs of 93.33% and 90.00%, respectively, while the traditional cosine similarity matching method has TARs of only 86.67% and 83.33%. It can be observed that our proposed scheme can largely resist the impact of static environment multipath changes. RF-Express, based on the neural network model, outperforms the traditional cosine similarity matching method, especially in dynamic multipath environments.

4) Impact of Conveyor Speed: Due to factors such as motor aging and varying weights of transported items, the conveyor speeds at the upstream and downstream nodes may differ. When designing the RF-Express system, we ensure an equal number of tag signal samples through interpolation. The following experiment tests the impact of different speeds on the system's true acceptance rate. We collect signal data for various items at five speed settings, ranging from speed level one (v1) to speed level five (v5), with speeds increasing from slow to fast. Using the signals collected at speed level three (v3) as the upstream samples, and signals at all five speed levels as the downstream samples, the results in Fig. 12 show that TARs reach 100% for speeds v1 to v4, with only speed v5 having a TAR of 91.67%. This indicates that the interpolation approach we adopted can successfully handle changes in speed. However, if the speed is too fast, resulting in too few collected samples, the accuracy may decrease.

5) Impact of Package-Antenna Distance: The package-antenna distance we refer here is defined as the vertical distance between the package and the antenna that is perpendicular to the direction of the conveyor belt. We aim to maintain the same package-antenna distance for different nodes by accurately setting the location of the antenna and allowing the package to move along the edge of the sorting table. However, in reality, factors such as package deformation can still cause some distance variations. In this section, we experimentally test the system's true acceptance rate under different distance settings. We collect upstream signal samples at a specific package-antenna distance. Under four different distance variations, we collect downstream sample data, based on moving forward by $1.0\,\mathrm{cm}$, moving forward by $3.0\,\mathrm{cm}$, moving backward by $1.0\,\mathrm{cm}$, and moving backward by $3.0\,\mathrm{cm}$ from the original specific distance (forward and backward respectively represent a decrease and increase in the package-antenna distance). The results are depicted in Fig. 13. The downstream samples under the four distance variations achieve

TARs of 90.91%, 81.82%, 100%, and 63.64%, respectively. This indicates that RF-Express can resist the impact of package-antenna distance variations to some extent. However, if the distance change is too large, the performance of the system will still be affected.

6) Impact of Item's Movement: During transportation, external impacts that are too strong may occur. At such circumstances, it is challenging to maintain the position of items inside the package completely. Lateral and vertical orientations represent directions parallel and perpendicular to the conveyance direction, respectively. We collect upstream sample data when the item was in the center of the package. Then we move the item laterally and vertically by $0.5\,\mathrm{cm}$, $1.0\,\mathrm{cm}$, $2.0\,\mathrm{cm}$, $3.0\,\mathrm{cm}$, and $5.0\,\mathrm{cm}$, respectively, and collect the signal data for these movement scenarios as downstream samples. The results, as shown in Fig. 14 and Fig. 15, indicate that the correct acceptance rates for these five lateral movement scenarios are 100%, 91.67%, 41.67%, 16.67%, and 0%, respectively, while for vertical movement, they are 91.67%, 83.33%, 75.00%, 66.67%, and 33.33%. It can be observed that minor item movement has a relatively small impact on the system, and the impact of the same distance of vertical movement on the system is slightly smaller.

VI. Related Work

A. RFID-based Sensing

Establishing a relationship model between RF signals and perceived objects enables robust target feature sensing. Researchers have conducted a series of explorations and achieved multiple breakthroughs in various aspects such as material identification, human sensing, and environmental sensing [20]–[22].

Material Identification: Tagtag [23] utilizes the property that the tag antenna impedance changes with the type of target material, and uses the phase change associated with impedance for material sensing. In [24], researchers design an efficient feature extraction model, utilizing the phase change of the combined received signal to infer the strength of reflection signal, thereby achieving material recognition.

Human Sensing: Hand-Key [25] uses an RFID tag array to collect the inner body composition and outer geometry features of a person's hand to identify the user. When the human fingers touch the surface of an RFID tag, antenna impedance changes, manifesting as phase changes in the tag's backscatter signal. Early attempt in [26] utilizes this phenomenon for a touch-sensitive application. BioDraw [27] employs four categories of biometrics (impedance, geometry, behavior, and composition) of human hand, for a multi-factor user authentication method.

Environmental Sensing: RTSense [28] exploits the property of tag impedance changing with temperature to explore the feasibility of passive tags converting into battery-free temperature sensors. The work utilizing the tag's volatile memory in [29], measures the discharge period of a reverse-biased diode to indirectly estimate the environmental temperature of the RFID tag. GreenTag [30] attaches two RFID tags to a cultivation pot, reflecting changes in soil humidity through the proposed metric of differential minimum response threshold between the two tags.

B. RFID-based Authentication

With increasing adoption of RFID technology in the supply chain area, the security of RFID systems becomes a mandatory requirement for the transportation of expensive goods. Existing work on RFID authentication mainly falls into two categories: application-layer and physical-layer authentication.

Application-layer Authentication: Early researchers in [31] introduce an method for detecting cloned tags by writing random numbers to the tag, which can identify tags with the same EPC code in the same scenario. KTAuth [4] propose a lightweight authentication method that effectively detects lost and forged tags by utilizing a dedicated memory block that can be used to support read permission control.

Physical-layer Authentication: The work in [32] introduces a clone tag detection scheme based on the RSSI-phase profile, modeling tag signals in both static and dynamic scenes. ReaderPrint [33] utilizes the impedance mismatch degrees of different reader antennas across channels to realize an effective RFID reader authentication system. Butterfly [34] proposes a physical layer authentication approach with elasticity to environment and location by using the difference between the signals of two tags as their fingerprint.

Our work is inspired by the aforementioned efforts in utilizing RFID for sensing, aiming to detect the status of items inside packages by modeling radio frequency signals. Previous RFID-based authentication attempts primarily focus on verifying the authenticity of tags, lacking the capability to assess the actual conditions of the items. Therefore, we introduce a novel scheme, steering authentication towards the detection of the item status, with the goal of promptly identifying anomalies.

VII. Conclusion

Focusing on the field of smart logistics, this work introduces, for the first time, a non-intrusive and highly robust commodity authentication method based on RFID, with purely commercial devices and almost without additional costs. By trickily deploying a pair of tags on each package, we effectively mitigate the adverse effects of environmental multipath changes on the authentication performance. Additionally, a feature matching algorithm based on triplet network is employed to enhance the robustness of the system. A prototype of RF-Express has been implemented in a real lab environment and experimental evaluations demonstrate a mean TAR and TRR of 90.97% and 94.38%, respectively. We believe that RF-Express will open up more possibilities for practical commodity authentication and anti-counterfeiting technologies in modern supply chains.

Acknowledgments

This research is supported in part by the National Natural Science Foundation of China (Grants No. 62372045 and No. 62072040) and the Beijing Institute of Technology Research Fund Program for Young Scholars.

REFERENCES

[1] T. Zhu and J. Wang, "Study on the service quality of express logistics based on the satisfaction of international students a sample of chinese students studying in south korea," in *Proceedings of the 3rd International Conference on Judicial, Administrative and Humanitarian Problems of State Structures and Economic Subjects (JAHP)*, pp. 375–379, 2018.

[2] J. Di and H. Liang, "Research on express service based on improving customer satisfaction," in *Proceedings of the MATEC Web of Conferences*, p. 03003, 2020.

[3] I. M. D. Priyanto, I. M. Sarjana, and I. M. Subaw, "Implementation of article 18 of the consumer protection law in express delivery companies in denpasar city, indonesia," *Path of Science*, vol. 9, no. 8, pp. 1019–1029, 2023.

[4] X. Xie, X. Liu, S. Guo, H. Qi, and K. Li, "A lightweight integrity authentication approach for rfid-enabled supply chains," in *Proceedings of the IEEE International Conference on Computer Communications (INFOCOM)*, pp. 1–10, 2021.

[5] M. Safkhani, S. Rostampour, Y. Bendavid, and N. Bagheri, "Iot in medical & pharmaceutical: Designing lightweight rfid security protocols for ensuring supply chain iintegrity," *Computer Networks*, vol. 181, p. 107558, 2020.

[6] W. Wang, A. Sadeqi, H. R. Nejad, and S. Sonkusale, "Cost-effective wireless sensors for detection of package opening and tampering," *IEEE Access*, vol. 8, pp. 117122–117132, 2020.

[7] G. Wang, J. Han, C. Qian, W. Xi, H. Ding, Z. Jiang, and J. Zhao, "Verifiable smart packaging with passive rfid," *IEEE Transactions on Mobile Computing*, vol. 18, no. 5, pp. 1217–1230, 2019.

[8] L. Yang, Q. Lin, X. Li, T. Liu, and Y. Liu, "See through walls with cots rfid system!," in *Proceedings of the 21st Annual International Conference on Mobile Computing and Networking (MobiCom)*, pp. 487–499, 2015.

[9] D. Vasisht, G. Zhang, O. Abari, H.-M. Lu, J. Flanz, and D. Katabi, "In-body backscatter communication and localization," in *Proceedings of the Conference of the ACM Special Interest Group on Data Communication (SIGCOMM)*, pp. 132–146, 2018.

[10] W. Xu, J. Liu, S. Zhang, Y. Zheng, F. Lin, J. Han, F. Xiao, and K. Ren, "Rface: Anti-spoofing facial authentication using cots rfid," in *Proceedings of the IEEE International Conference on Computer Communications (INFOCOM)*, pp. 1–10, 2021.

[11] L. Tsang, J. A. Kong, and R. T. Shin, "Theory of microwave remote sensing," 1985.

[12] C. Duan, J. Liu, X. Ding, Z. Li, and Y. Liu, "Full-dimension relative positioning for rfid-enabled self-checkout services," *Proceedings of the ACM on Interactive, Mobile, Wearable and Ubiquitous Technologies*, vol. 5, no. 1, pp. 1–23, 2021.

[13] C. Wang, J. Liu, Y. Chen, H. Liu, L. Xie, W. Wang, B. He, and S. Lu, "Multi-touch in the air: Device-free finger tracking and gesture recognition via cots rfid," in *Proceedings of the IEEE International Conference on Computer Communications (INFOCOM)*, pp. 1691–1699, 2018.

[14] F. Schroff, D. Kalenichenko, and J. Philbin, "Facenet: A unified embedding for face recognition and clustering," in *Proceedings of the IEEE Conference on Computer Vision and Pattern Recognition (CVPR)*, pp. 815–823, 2015.

[15] Q. Feng, P. Li, Z. Lu, Z. Zhou, Y. Wu, J. Weng, and F. Huang, "Dhan: Encrypted jpeg image retrieval via dct histograms-based attention networks," *Applied Soft Computing*, vol. 133, p. 109935, 2023.

[16] H. Luo, W. Jiang, Y. Gu, F. Liu, X. Liao, S. Lai, and J. Gu, "A strong baseline and batch normalization neck for deep person re-identification," *IEEE Transactions on Multimedia*, vol. 22, no. 10, pp. 2597–2609, 2020.

[17] EPCglobal, "Low level reader protocol (llrp)," 2010.

[18] A. Paszke, S. Gross, F. Massa, A. Lerer, J. Bradbury, *et al.*, "Pytorch: An imperative style, high-performance deep learning library," *Advances in Neural Information Processing Systems (NeurIPS)*, vol. 32, pp. 8026–8037, 2019.

[19] D. P. Kingma and J. Ba, "Adam: A method for stochastic optimization," *arXiv preprint arXiv:1412.6980*, 2014.

[20] F. Shang, P. Yang, J. Xiong, Y. Feng, and X. Li, "Tamera: Contactless commodity tracking, material and shopping behavior recognition using cots rfids," *ACM Transactions on Sensor Networks*, vol. 19, no. 2, pp. 1–24, 2023.

[21] Y. Zhu, C. Duan, X. Ding, and Z. Yang, "Rosense: Refining los signal phase for robust rfid sensing via spinning antenna," *IEEE Internet of Things Journal*, vol. 9, no. 23, pp. 24135–24147, 2022.

[22] A. Huang, D. Wang, R. Zhao, and Q. Zhang, "Au-id: Automatic user identification and authentication through the motions captured from sequential human activities using rfid," *Proceedings of the ACM on Interactive, Mobile, Wearable and Ubiquitous Technologies*, vol. 3, no. 2, pp. 1–26, 2019.

[23] B. Xie, J. Xiong, X. Chen, E. Chai, L. Li, Z. Tang, and D. Fang, "Tagtag: Material sensing with commodity rfid," in *Proceedings of the 17th Conference on Embedded Networked Sensor Systems (SenSys)*, pp. 338–350, 2019.

[24] Z. Chen, P. Yang, J. Xiong, Y. Feng, and X.-Y. Li, "Tagray: Contactless sensing and tracking of mobile objects using cots rfid devices," in *Proceedings of the IEEE International Conference on Computer Communications (INFOCOM)*, pp. 307–316, 2020.

[25] J. Liu, X. Zou, F. Lin, J. Han, X. Xu, and K. Ren, "Hand-key: Leveraging multiple hand biometrics for attack-resilient user authentication using cots rfid," in *Proceedings of the IEEE 41st International Conference on Distributed Computing Systems (ICDCS)*, pp. 1042–1052, 2021.

[26] S. Pradhan, E. Chai, K. Sundaresan, L. Qiu, M. A. Khojastepour, and S. Rangarajan, "Rio: A pervasive rfid-based touch gesture interface," in *Proceedings of the 23rd Annual International Conference on Mobile Computing and Networking (MobiCom)*, pp. 261–274, 2017.

[27] J. Liu, X. Zou, J. Han, F. Lin, and K. Ren, "Biodraw: Reliable multi-factor user authentication with one single finger swipe," in *Proceedings of the IEEE/ACM 28th International Symposium on Quality of Service (IWQoS)*, pp. 1–10, 2020.

[28] S. Pradhan and L. Qiu, "Rtsense: Passive rfid based temperature sensing," in *Proceedings of the 18th Conference on Embedded Networked Sensor Systems (SenSys)*, pp. 42–55, 2020.

[29] X. Chen, J. Liu, F. Xiao, S. Chen, and L. Chen, "Thermotag: Item-level temperature sensing with a passive rfid tag," in *Proceedings of the 19th Annual International Conference on Mobile Systems, Applications, and Services (MobiSys)*, pp. 163–174, 2021.

[30] J. Wang, L. Chang, S. Aggarwal, O. Abari, and S. Keshav, "Soil moisture sensing with commodity rfid systems," in *Proceedings of the 18th International Conference on Mobile Systems, Applications, and Services (MobiSys)*, pp. 273–285, 2020.

[31] M. Lehtonen, D. Ostojic, A. Ilic, and F. Michahelles, "Securing rfid systems by detecting tag cloning," in *Proceedings of the 7th International Conference on Pervasive Computing*, pp. 291–308, 2009.

[32] X. Chen, J. Liu, X. Wang, X. Zhang, Y. Wang, and L. Chen, "Combating tag cloning with cots rfid devices," in *Proceedings of the 15th Annual IEEE International Conference on Sensing, Communication, and Networking (SECON)*, pp. 1–9, 2018.

[33] Y. Zhu, C. Duan, X. Ding, and Z. Yang, "Readerprint: A universal method for rfid readers authentication based on impedance mismatch," in *2022 19th Annual IEEE International Conference on Sensing, Communication, and Networking (SECON)*, pp. 352–360, 2022.

[34] J. Han, C. Qian, Y. Yang, G. Wang, H. Ding, X. Li, and K. Ren, "Butterfly: Environment-independent physical-layer authentication for passive rfid," *Proceedings of the ACM on Interactive, Mobile, Wearable and Ubiquitous Technologies*, vol. 2, no. 4, pp. 1–21, 2018.